

Article

Evaluation of Structural Changes in the Coal Specimen Heating Process and UCG Model Experiments for Developing Efficient UCG Systems

Faolang Su ¹, Takuya Nakanowataru ¹, Ken-ichi Itakura ^{1,*}, Koutarou Ohga ²
and Gota Deguchi ³

¹ Graduate School of Engineering, Muroran Institute of Technology, 27-1 Mizumoto, Muroran 050-8585, Japan; E-Mails: sfqmuroran@gmail.com (F.S.); s1923072@mmm.muroran-it.ac.jp (T.N.)

² Graduate School of Engineering, Hokkaido University, Kita-ku, Sapporo 060-8628, Japan; E-Mail: k-ohga@eng.hokudai.ac.jp

³ Underground Resources Innovation Network, NPO, Higashi-ku, Sapporo 007-0847, Japan; E-Mail: gota@mue.biglobe.ne.jp

* Author to whom correspondence should be addressed; E-Mail: itakura@mmm.muroran-it.ac.jp; Tel.: +81-143-46-5424; Fax: +81-143-46-5499.

Received: 6 February 2013; in revised form: 2 April 2013 / Accepted: 23 April 2013 /

Published: 3 May 2013

Abstract: In the underground coal gasification (UCG) process, cavity growth with crack extension inside the coal seam is an important phenomenon that directly influences gasification efficiency. An efficient and environmentally friendly UCG system also relies upon the precise control and evaluation of the gasification zone. This paper presents details of laboratory studies undertaken to evaluate structural changes that occur inside the coal under thermal stress and to evaluate underground coal-oxygen gasification simulated in an *ex-situ* reactor. The effects of feed temperature, the direction of the stratified plane, and the inherent microcracks on the coal fracture and crack extension were investigated using some heating experiments performed using plate-shaped and cylindrical coal specimens. To monitor the failure process and to measure the microcrack distribution inside the coal specimen before and after heating, acoustic emission (AE) analysis and X-ray CT were applied. We also introduce a laboratory-scale UCG model experiment conducted with set design and operating parameters. The temperature profiles, AE activities, product gas concentration as well as the gasifier weight losses were measured successively during gasification. The product gas mainly comprised combustible components such as CO, CH₄,

and H₂ (27.5, 5.5, and 17.2 vol% respectively), which produced a high average calorific value (9.1 MJ/m³).

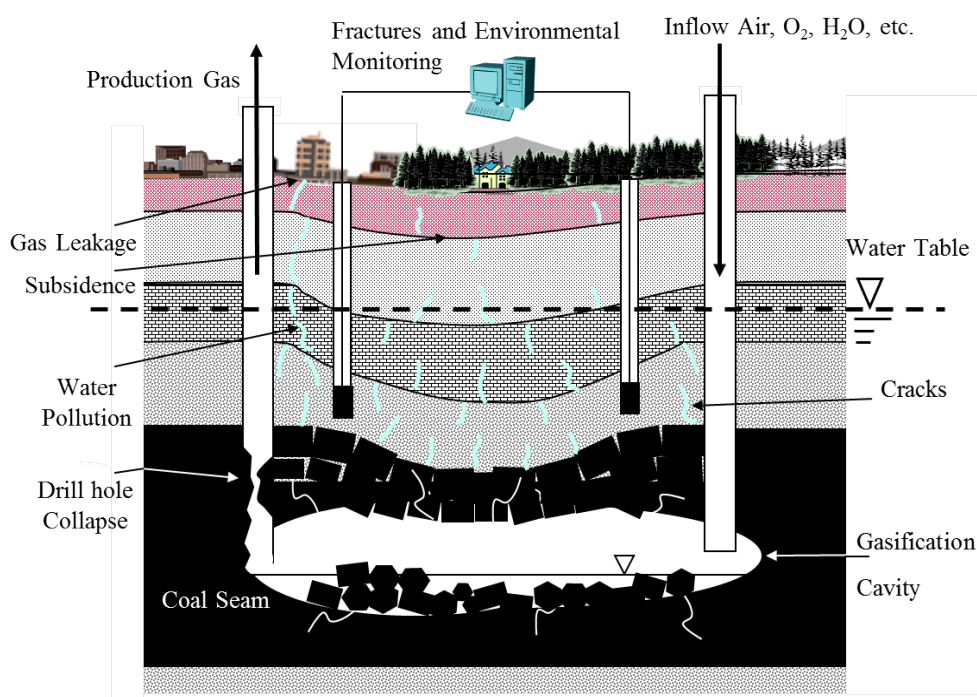
Keywords: coal fracture; crack extension; structural change; acoustic emission; underground coal gasification

1. Introduction

Coal, the largest fossil fuel energy resource, is the largest source of carbon dioxide emissions worldwide. The share of coal energy among all used energy resources will continue to grow [1]. Nevertheless, large quantities of these tremendous resources cannot be used effectively: thin and deep coal seams are not economic to extract. Furthermore, the production safety of traditional mining is a significant problem. Consequently, making better use of existing coal resources appears to be a particularly important issue.

As a clean coal technology, underground coal gasification (UCG) is a promising mode of coal recovery. Simply put, UCG is a technology for creating a combustion reactor in an underground coal seam that converts coal *in situ* into a gaseous product such as synthesis gases (hydrogen, methane, *etc.*) through the same chemical reactions that occur in surface gasifiers. A typical closed UCG system is presented in Figure 1. It includes a coal seam with two boreholes drilled down into it: one for injecting air or oxygen for *in-situ* burning of coal and the other to extract the gaseous products.

Figure 1. Diagram of the UCG process with monitoring system.



The original idea of UCG was conceived by the British scientist Sir William Siemens and further advanced by the Russian chemist Dmitri Mendeleev [2,3]. In 1909, the first patent for UCG was

granted to Betts [4]. The first plan for an UCG trial was proposed by a Nobel Laureate-Sir William Ramsay, and it was prepared near Durham (UK) in 1912 [2,5]. Subsequently, theoretical and experimental research with *in-situ* UCG trials were started in the 1930s in the USSR and developed later in the US, Europe, Australia, and China, *etc.* [2–14]. Many countries have recently shown interest in this method because modern sensing and control techniques can reduce UCG impact on the Earth's environment by limiting greenhouse gas emissions to the air and by producing no ash on the surface. Recently, UCG has also been regarded as a potential technology for production of hydrogen at a competitive price compared to other purification technologies [15–17] and for the use of partially abandoned mines [18–20].

Most problems that might occur with UCG, such as subsidence, gas leakage, and groundwater pollution, are caused by fractures near the combustion area. Furthermore, the efficiency of coal combustion is not high compared with that of other coal mining methods. Precise control of the combustion reactor is difficult because the techniques to evaluate and control the fracturing activity in the coal seam around the combustion area remain undeveloped. Therefore, fracturing inside the coal under a heating process is important to evaluate and control coal gasification *in-situ* because enlargement of the free surface around a linking hole with cracking inside the coal seam directly influences the gasification efficiency.

Based on our earlier studies [21], in order to construct a secure and efficient UCG system, it is necessary to develop a reasonable design for expansion of the gasification zone and for effective control of the combustion area in the coal seam. We realized that the UCG cavity growth is an extremely complicated phenomenon associated with coal fracturing operating parameters and other geological agents. Accordingly, the present work specifically examines internal structure changes of a coal specimen under different term-settings and investigates the effects of the direction of the fire surface and coal stratified plane on crack generation.

In addition, progress in UCG deployment has been hampered by insufficient modeling methodology and a lack of understanding of its quantitative physical processes [22]. The need exists to obtain experimental data of cavity growth and gasification effects with respect to a given set of design and operating parameters. Consequently, in this paper, we introduced a laboratory-scale experiment conducted using an *ex-situ* UCG reactor.

In the present work, acoustic emission (AE) techniques were applied to monitor the evolution of fracture inside the coal samples. AE sensors with waveguides were put on/inside the coal specimens and an UCG reactor. In our earlier studies, point heating experiments using CO₂ lasers were done to verify the generation of AEs with the heating processes of coal and coal-rock [23]. The results obtained from the series of experiments showed that coal generated AEs with special AE activity patterns by the action of thermal stress. However, rock, sandstone, and shale never emitted AEs in the same process. It can be confirmed that AE monitoring is applicable for evaluation of coal damage and combustion zone propagation during the gasification process.

2. Structural Change Estimation in Coal Specimen

2.1. Experimental Apparatus and Procedure

To simplify the measurement and monitoring of heating process, plate-shaped and cylindrical coal specimens were used for this study. The coal samples were prepared by cutting them from coal blocks that had been produced at the Kushiro Coal Mine, Japan and at some coal seams in Canada. When the coal was cut, the coal block was covered with plaster to prevent its disintegration. The specimens were collected along the parallel and vertical direction of the stratified plane at different locations within the coal block to ensure homogeneity. The result of the ultimate and proximate analysis of the coal which is used in the heating experiments is shown in Table 1. The coal samples used in the present works are of low sulfur (0.23%) content. At 15.40% the ash content is rather high. The typical dimensions of coal specimens and operating conditions used for these experiments are presented in Table 2.

Table 1. Proximate and ultimate analysis of coal samples.

No.	Parameter	Kushiro coal
Proximate analysis (%)		
1	Fixed moisture	5.30
2	Ash content	15.40
3	Volatile matter	40.10
4	Fixed carbon	39.20
5	Total sulfur	0.23
Ultimate analysis (%)		
6	Carbon	65.70
7	Hydrogen	5.99
8	Nitrogen	1.12
9	Oxygen	10.89

Table 2. Operating conditions and coal specimen dimensions.

No.	Coal types	Shape	Direction of stratified plane	Operation time (min)	Geometrical parameters (mm)		
					high	wide	thick
P1	Kushiro	Plate-shaped	vertical	127	40	20	5
P2	Kushiro	Plate-shaped	vertical	55	40	20	5
P3	Kushiro	Plate-shaped	horizontal	55	40	20	5
C1	Canada	Cylindrical	vertical	135	20	10 (diameter)	
C2	Canada	Cylindrical	vertical	45	20	10 (diameter)	

A schematic diagram of the experimental setup is shown in Figure 2. To detect microcracking noises coming from the coal, conical lead zirconate titanate (PZT) ceramic elements were used as AE sensors (see Figure 2). These piezoelectric sensors, with top diameter of 1 mm, bottom diameter of 4 mm, and height of 2 mm were cemented on the side surface of the specimens using heat-resistant cement. One AE signal was amplified up to 70 dB with a preamplifier and signal conditioner, and AE counts and events are recorded on a data logger (GL900; Graphtec Corp., Yokohama, Japan). In this measurement system, AE events show the number of microcracking noises: AE count reflects the

event magnitude. All AE waveforms from sensors were recorded using a multi-recorder (GR-7000; Keyence Co., Osaka, Japan) with sampling time of 500 ns.

To investigate the microcrack distribution inside the coal specimen, 3D CT images obtained before and after specimen heating were recorded using a micro-focus X-ray CT (1174; (SkyScan, Bruker MicroCT, Kontich, Belgium). The specification parameters are presented in Table 3.

Figure 2. (a) Experimental setup for coal specimen heating; (b) AE sensor characteristics.

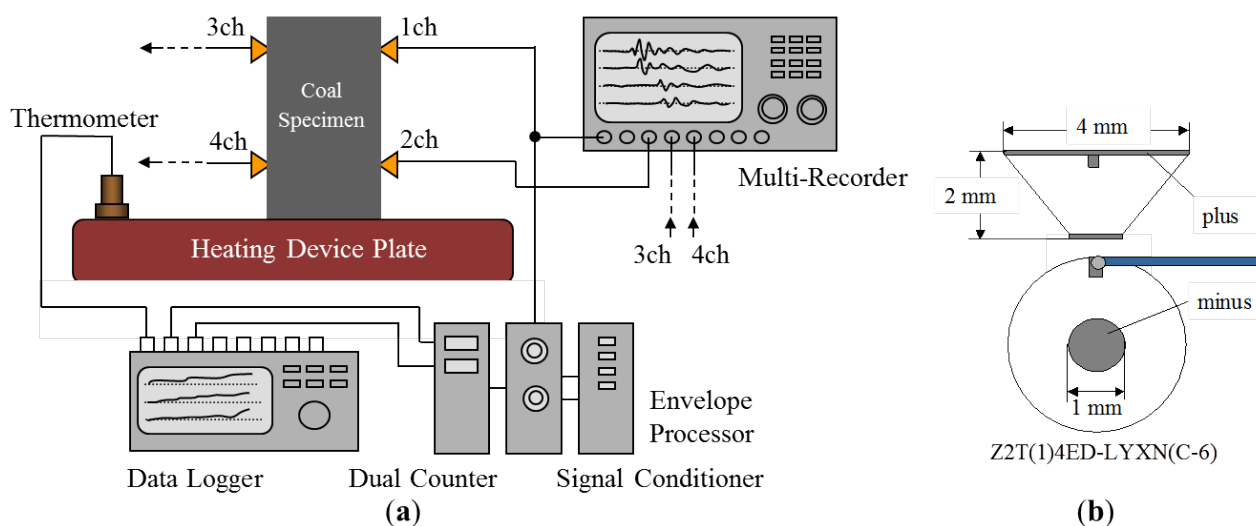
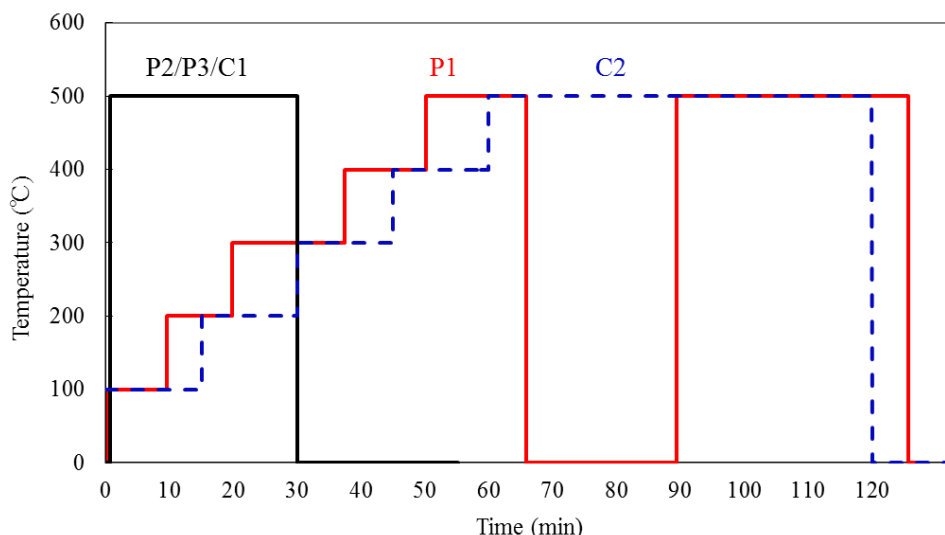


Table 3. Specifications of X-ray CT (1174; SkyScan/Bruker MicroCT).

Specification	Description
Spatial resolution	voxel size (6–30 μm), low-contrast resolution (10 μm)
X-ray Source	Sealed air-cooled x-ray tubes 20–50 kV, 40 W
X-ray Detector	1.3 M pixels (1280 \times 1024), 12 bit CCD
Sample maximum size	Diameter (5–30 mm), Length (50 mm), Height (50 mm)
Reconstruction Algorithm	Feldkamp algorithm with volumetric (cone-beam) geometry
Installation requirements	Temperature (18–25 $^{\circ}\text{C}$), no condensation, <85% humidity

For controlling the heating temperature, the bottom face of the specimen was heated to a certain temperature at designated time intervals. The temperatures of the P1 test were 0–500 $^{\circ}\text{C}$, changing by 100 $^{\circ}\text{C}$ for every step in the earlier stage. Cooling lasted 25 min before the maximum setting temperature (500 $^{\circ}\text{C}$). To elucidate the booming temperature change, the P2 specimen was heated to 500 $^{\circ}\text{C}$ from the beginning of the experiment, with the temperature maintained for 30 min, as shown in Figure 3. Stratified planes in these two tests are perpendicular to the heating surface. For comparison, the P3 test was performed under the same temperature conditions as P2, but the heating surface in this case is parallel to the stratified planes.

Figure 3. Temperature loading procedures.



2.2. Heating Experiments of Plate-Shaped and Cylindrical Specimens

Figure 4 presents AE count rates, events obtained during the heating process. The surface temperature changes of heater detected by the temperature sensor are shown. Results show that the AE activity increased considerably when the surface temperature of the specimen changed, especially for the large temperature gradient. After the experiment, many microcracks were observed on the specimen surface. These AEs were generated with crack generation and developments inside the specimen.

Figure 4. Temperature variation and AE activity monitored in the process of (a) P1; and (b) P2 tests.

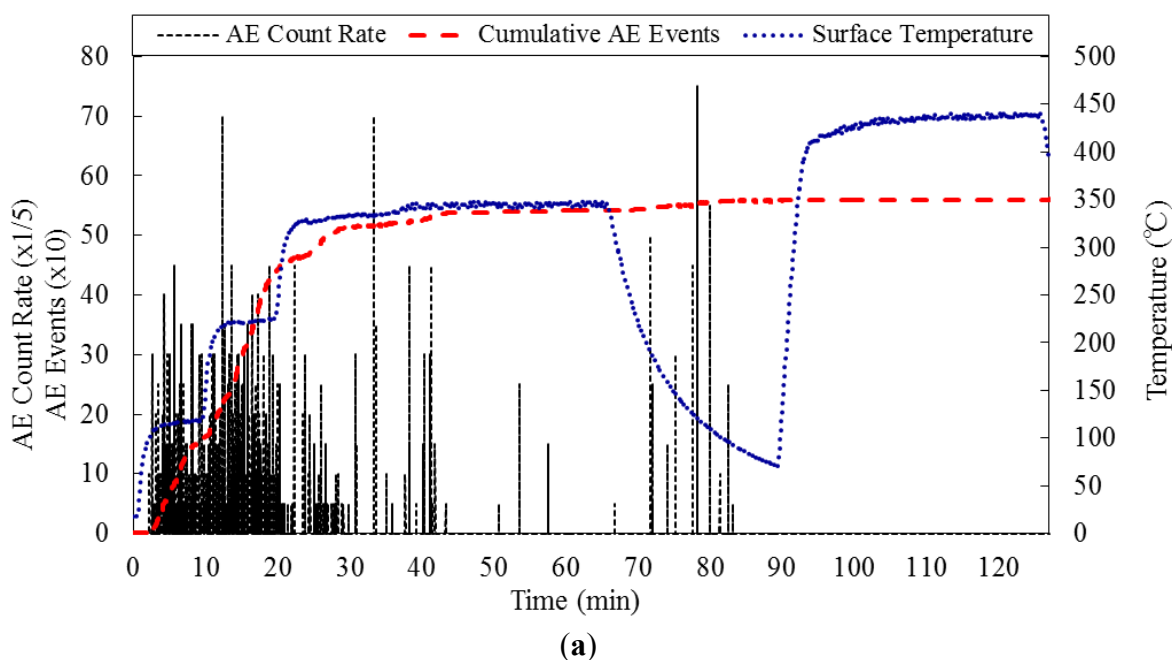


Figure 4. Cont.

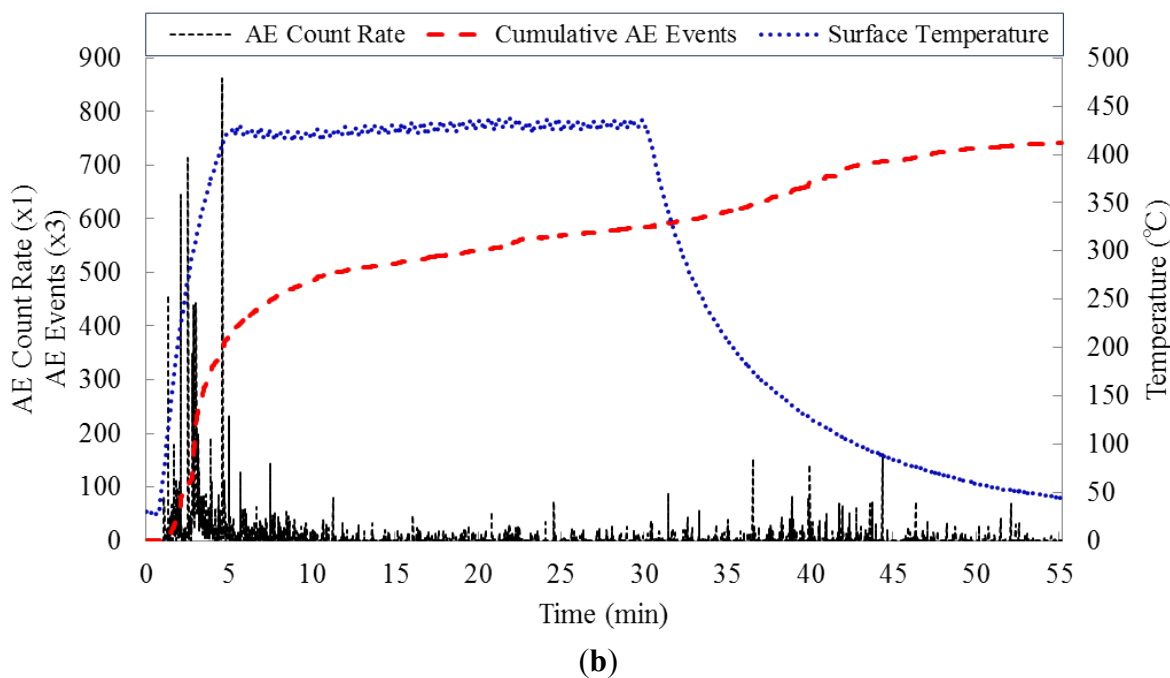


Figure 5 shows 3D CT images obtained before and after these three specimens' heating. Results show that many microcracks developed inside the specimen, especially at the bottom; then the crack density changed. The angles (0° – 10°) of generated cracks were quantified, indicating the fracture progress direction inside the coal specimens, as shown in Figure 6. Comparison of the P1 and P2 tests showed a different heating process with the different setting temperature; it is apparent that plenty of microcracks occurred in the vicinity of heating surface. In addition, with respect to the P1 test, the P2 specimen generated fewer microcracks and had a much larger trend to crack during the rapid heating process. To quantify these structural changes, we investigated the fissure number (Figure 7) and volume (Figure 8) distribution within 30 mm distance from the heating surface of the coal specimens, as detected in 3D CT images. Moreover, correlation between the fissure number and crack volume was obtained (Figure 9).

Figure 5. Internal cracks generated inside the coal specimens [(a) P1; (b) P2; and (c) P3] before and after heating.

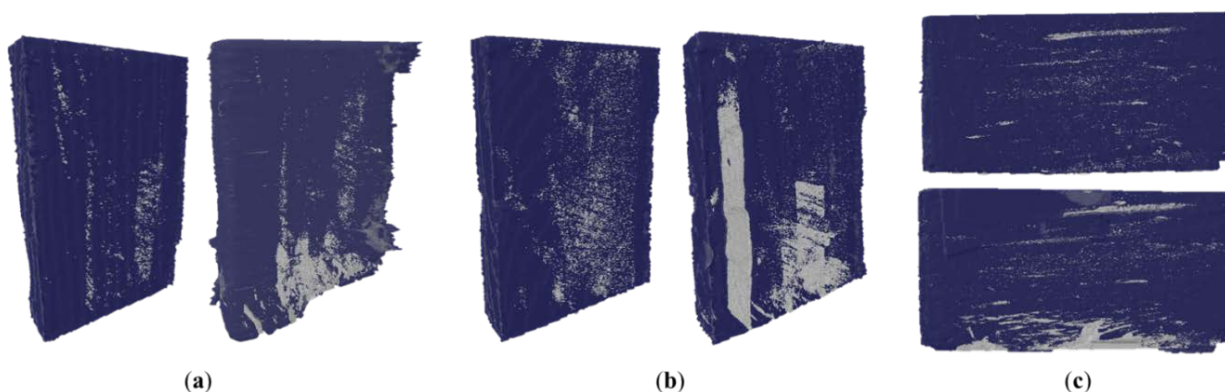


Figure 6. Crack angles inside the coal specimens ((a) P1; (b) P2; and (c) P3) after heating.

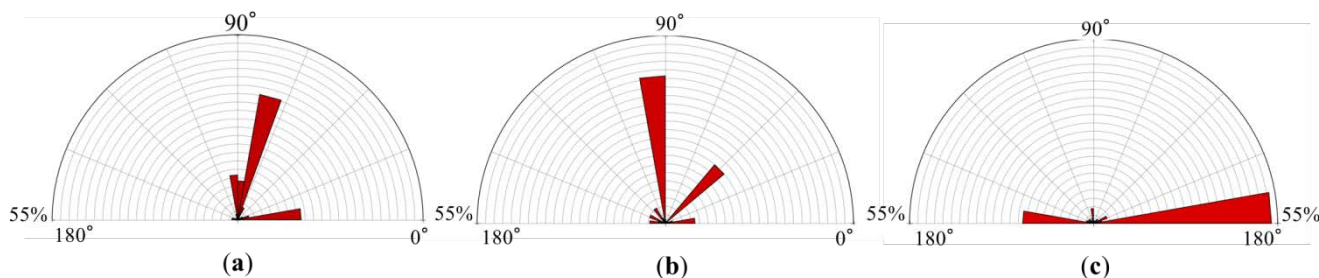


Figure 7. Microcrack distribution along the specimen height of (a) P1; and (b) P2.

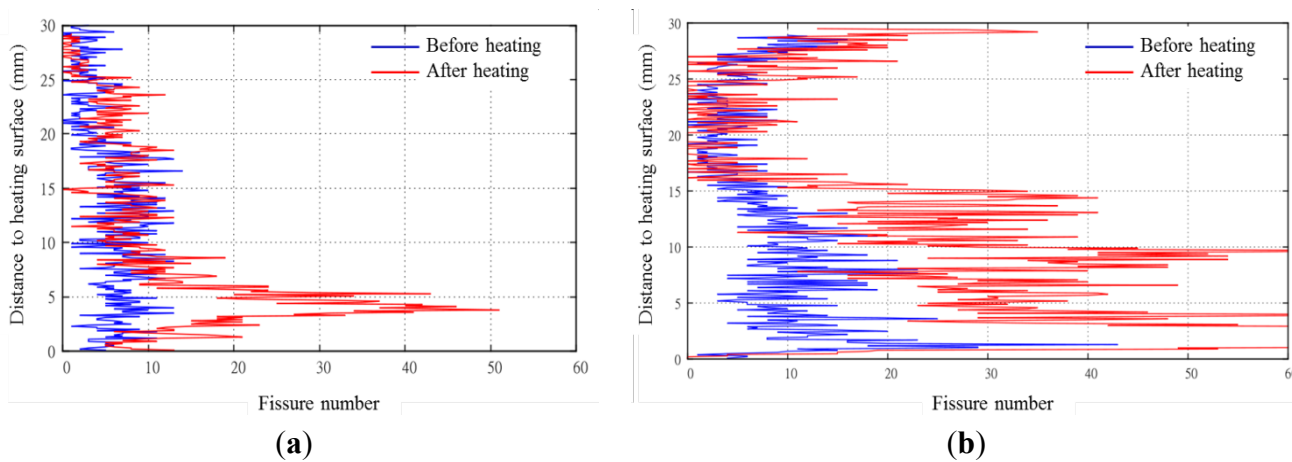
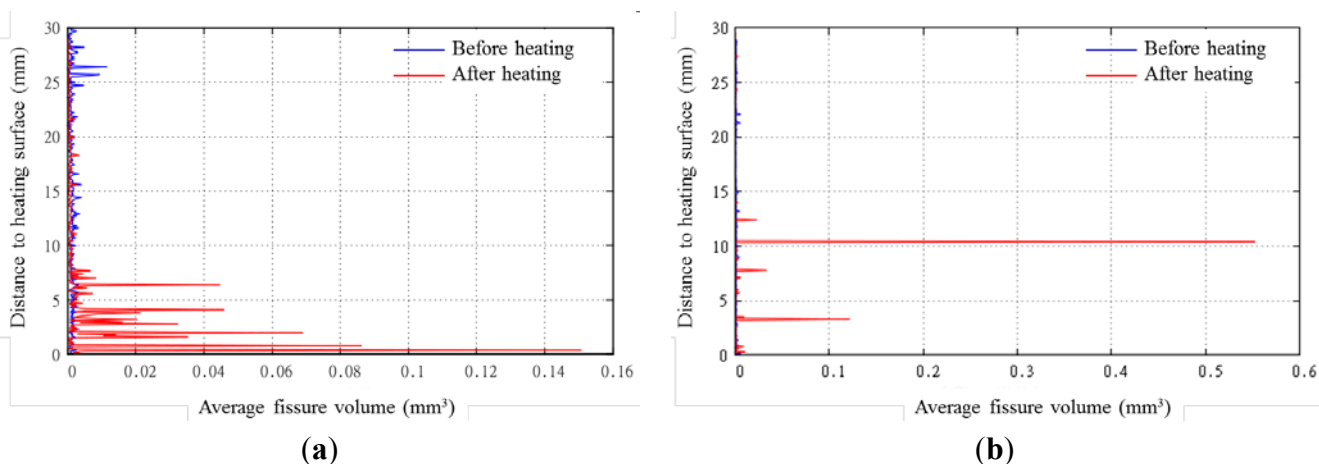


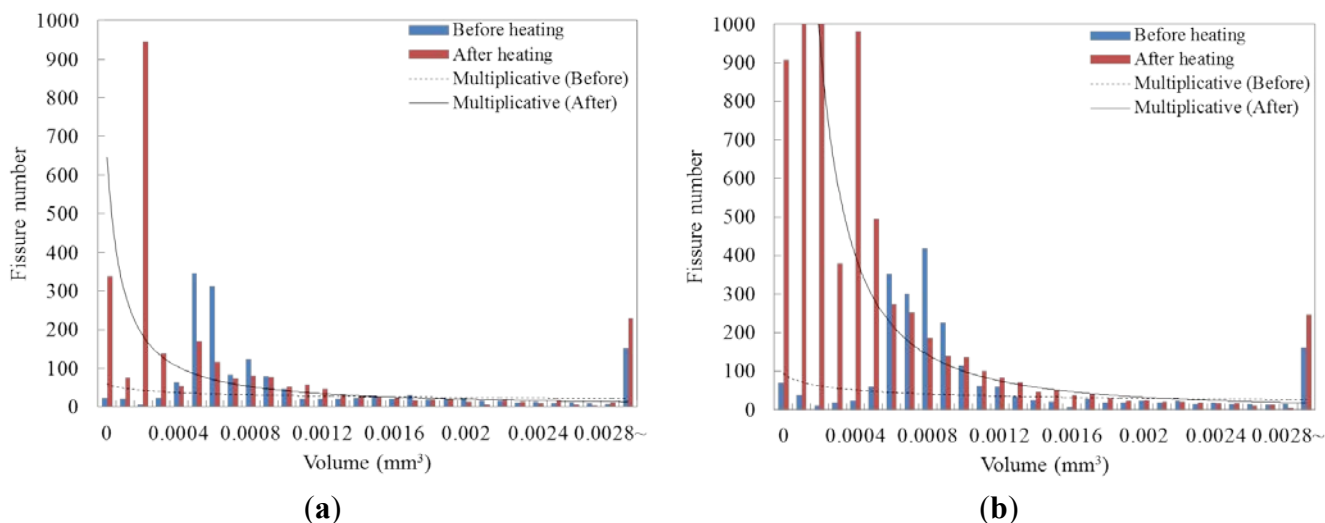
Figure 8. Average fissure volume along the specimen height of (a) P1; and (b) P2.



Most cracks are concentrated in a range of 0–8 mm in the bottom area of the P1 test and internal density also is low, with an average fissure volume distribution. The fractures occurring in the P2 specimen are distributed almost throughout the whole region, demonstrating that the thermal gradient of the specimen induced thermal stress. Subsequently, microcrack initiation and extension occurred. Furthermore, the transition of the thermal decomposition area with coal gasification partially alters the specimen density. Aside from affecting the average fissure volume distribution with big cracks, the fissure number near the heating surface also tends to rise on the whole. Furthermore, more and greater

microcracks formed after the experiment in the P1 coal specimen, as the approximate curve in Figure 9 shows, which is mainly the result of the greater temperature gradient used during the heating process.

Figure 9. Relation of fissure number and average fissure volume in the (a) P1; and (b) P2 test.



The *in-situ* permeability of the coal is an important factor for an efficient gasification and can be enhanced under the high temperature field. Herein, even though we had not obtained the available permeability variation data, the porosity factor of these specimens was obtained through the information provided by 3D CT images, taken before and after the heating process. The porosities of coal specimens P1, P2 before the experiments, were 5.53% and 8.08%. After the different heating processes, these porosities increased to 12.69% and 28.97%, respectively. We can see that the porosity of the coal had changed after a heating process, especially for the specimen P2 with high temperature gradients.

In addition, for investigation of the influence of inherent cracks and stratified plane direction in the coal samples, we collected and compared results of X-ray CT measurements and crack angle data from the P2 and P3 tests conducted using the same temperature settings. The only difference is that the stratified plane of the P3 coal specimen is parallel to the heating surface. Results show that the crack extension occurs along the longitudinal and horizontal directions, as shown in Figure 6. The crack propagation direction probably depends on the inherent microcracks, inclusions (calcite, *etc.*) and stratified plane direction.

A few experiments were conducted independently to support the obtained results with cylindrical coal samples under similar operating parameters. The cylindrical coal samples used in these works were collected from a deeply buried coal seam (about 1,400 m) in Canada. The loading procedures of heating temperature are presented in Figure 3. Figure 10 presents results of tests C1 and C2. For each result, the stratified plane is set on the heater and perpendicular to the heating surface. The results of the fissure number and average fissure number distribution as well as X-ray CT measurements are given in Figures 11 and 12. Similar results are shown in the 3D CT images. The generated microcrack assessments under sharply increased and incremental heating conditions are also shown.

Figure 10. Temperature variation and AE activity monitored in the process of (a) C1; and (b) C2 tests.

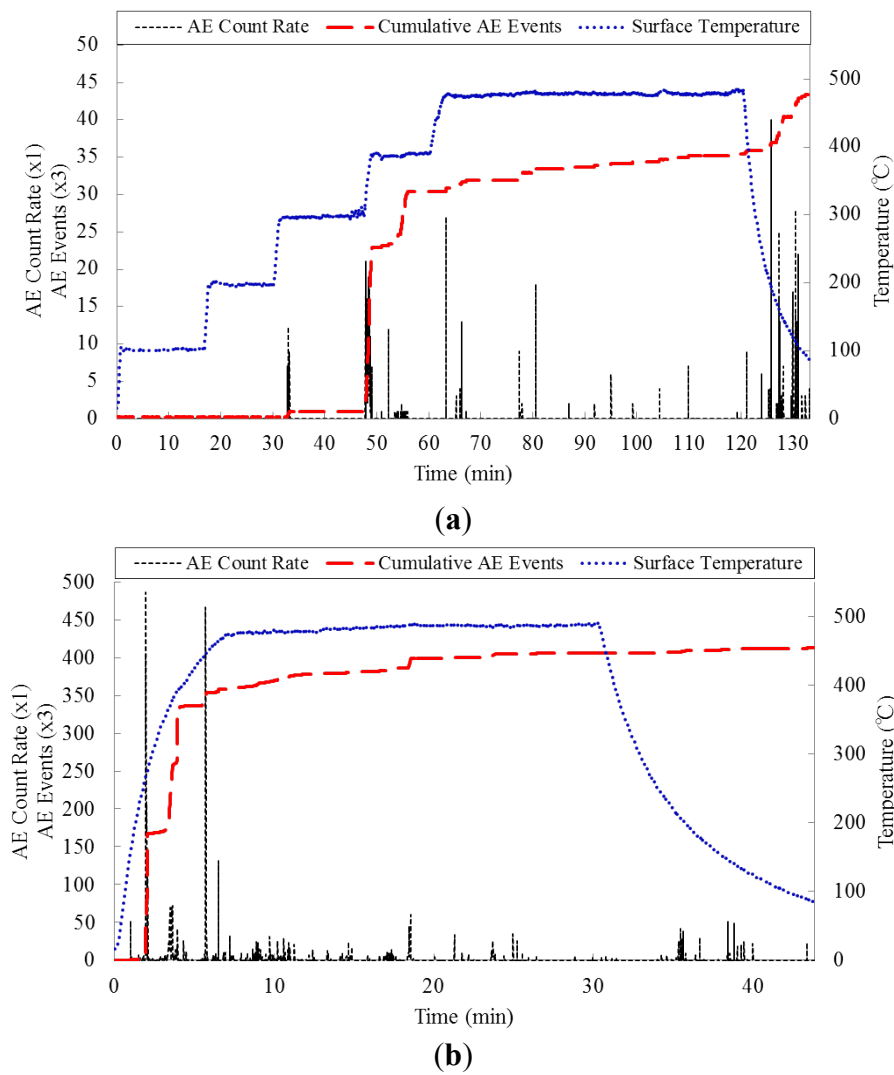


Figure 11. Internal cracks generated inside the coal specimens [(a) C1 and; (b) C2] before and after heating.

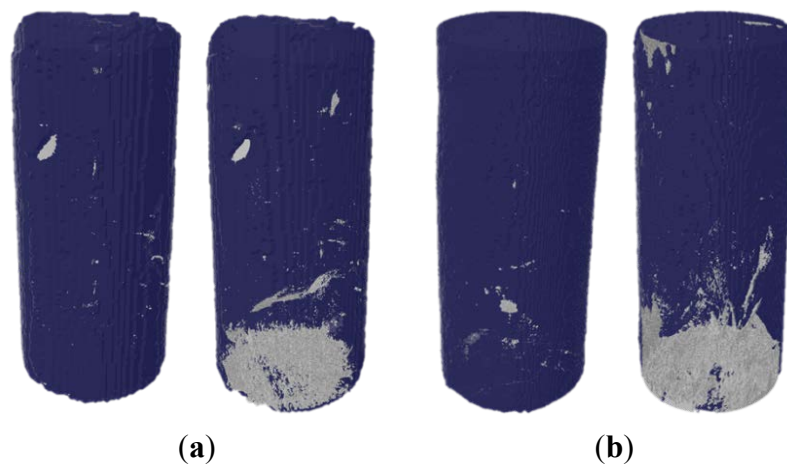
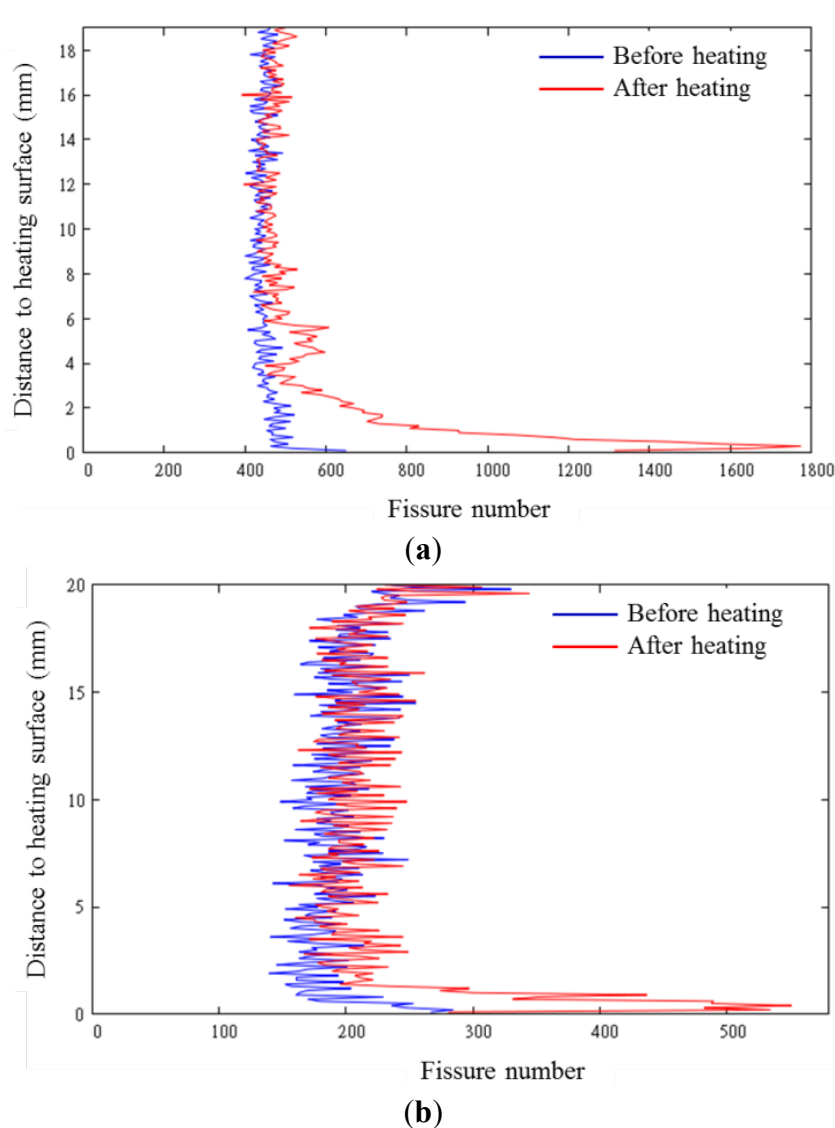


Figure 12. Microcrack distribution along the specimen height of (a) C1; and (b) C2.

In this work, the coal sample heating tests demonstrated that variations in material microcracks, porosity, and breakage are attributable to the distinct local thermal stress during the heating process. Results also show structural changes inside the coal specimen.

3. UCG Model Experiments

As seen in the results reported above, heating experiments performed on coal specimens demonstrate that microcracks tend to be larger and greater over the heating time. Typically, an off-width fracture is likelier to emerge with a high rate of change in the feeding temperature. It is also apparent that the direction of the stratified plane to the heating surface is a key factor for studying the UCG because the rate of crack extension directly influences the gasification process. Positive correlation was found between the temperature change and AE activities.

We manufactured a laboratory-scale UCG reactor that is applied in a single experiment with a V-shape linking-hole. According to the results obtained above, the gasification zone may be expanded more easily if the fire front is along the direction of the stratified plane of coal. Therefore, the

linking-hole (gasification channel) was drilled parallel to and as closely as possible to the stratified plane in the coal block. To provide a sufficient temperature field and sustain the gasification process, oxygen was used as the gasification agent. The AE monitoring and temperature measurement were applied for evaluating and controlling the gasification zone.

3.1. Experimental Design

The model design is viewed as the key step for the feasibility study, providing a reliable reference of the gasification process on the field scale. In a typical UCG process, two boreholes are drilled into the coal seam, connected by an underground gasification gallery created using various linking techniques [24–26] at proper distance apart. With development of the UCG technology, plenty of design approaches have taken place in the structure of the underground reactor. An underground reactor is created, which expands around the linking-hole, *i.e.*, the gasification channel.

An appropriate linking technique or drilling method is governed by the hydrogeological conditions, coal and surrounding rock properties (such as permeability, strength, thermal conductivity, *etc.*). Generally, the link between the two wells is required because the *in-situ* properties of the coal seam cannot meet the gas flow needs required for efficient gasification. Stream gasification is regarded as a reliable method, which had been successfully applied in many UCG trials, such as the Lisichansk, Leninsk and Gorlovka experiments, *etc.* [3,27]. Alexander [2] discussed this stream method in detail and also pointed out some disadvantages and other processing methods. Based on the stream method idea, more effective UCG ways were developed with the development of the long-distance well-linking technology. The high pressure break-up of the coal, hydro-fracturing, electric-linkage, linked vertical wells (LVW), former combustion linkage (FCL), and reverse combustion linkage (RCL) [5,28] were applied in the design and development of UCG. Since the 1980s, LLNL has developed an operational approach known as controlled retraction and injection point (CRIP) under the technology of directional underground drilling [5,9,29,30]. Based on the early USSR trials, the ϵ UCG [31] technology which relies on making use of the natural pathways and abandoned galleries that already exist in a coal seam and developing them further was also successfully used in the Chinchilla project (Australia).

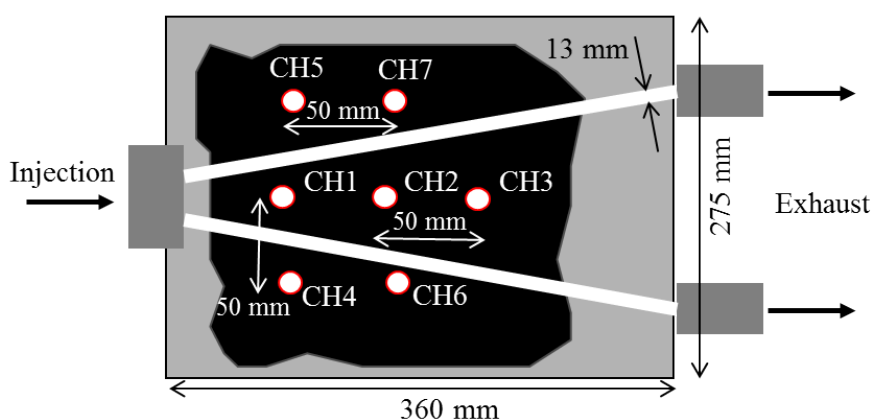
Some previous UCG operations performed in the U.S. (Hoe Creek I, II, and III) resulted in contaminated ground water because the organic combustion products were introduced into the aquifer [32]. In fact, the ground water also has a great influence on underground cavity formation and quantities of product synthesis generated during an UCG operation. Because the water contained in the enclosing rocks or adjacent aquifers will influx into the gasification zone through the formed cracks, especially in the case of applying the operation of syngas suction [2], during the gasification process. Therefore, the effect of local ground water on the UCG needs to be taken into account.

Based on the previous studies of UCG designs, a laboratory model trial using a V-shape linking-hole was conducted in this study for investigating the gasification zone movement and the gasification efficiency under the experimental conditions.

3.2. Monitoring of the AE Activities and Temperature Profile

As reported before, acoustic emission (AE), a real-time monitoring technology, can detect and possibly identify damage mechanisms that occur during the heating process of coal specimens by analyzing AE parameters. However, both the AE count rate and event only display qualitatively the damage process and intuitively cannot reflect the fractures occurring in large structures. Therefore, we attempt to obtain the source location where the event sources occurred and confirm the fracturing zone. Thermocouples were installed into the coal block for controlling the temperature profiles that provide crucial information in terms of process control and cavity growth. The section and dimensions of the simulated coal seam are presented in Figure 13.

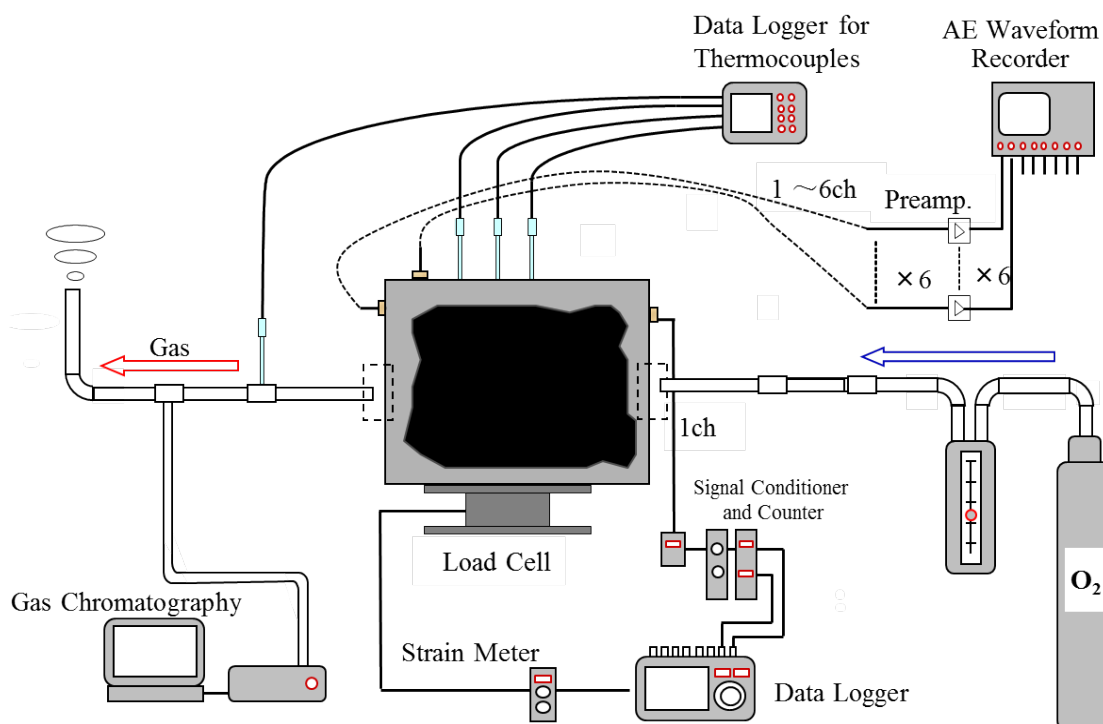
Figure 13. Dimensions and vertical cross-section of simulated UCG reactor.



3.3. Construction of the Simulated Seam with Coal Block

A coal block sample of roughly uniform size was obtained from the Kushiro Coal Mine (see Table 1). In the model, an irregular rectangular coal block was cast in the drum can ($\varnothing 27.5 \times 36$ cm) with heat-resistant concrete. A V-shaped 13×13 mm linking-hole was prepared inside the gasifier for injecting the gasification agent and exhausting the gas products. Figure 14 shows a schematic of the experimental set-up.

It is equipped with the gasification simulation reactor, a gas agent supply system, and a gas chromatographic analyzer for analyzing the product gas concentrations. A load cell was installed under the gasifier for recording the weight changes during the experiments. The drain tank was mounted at the gas production hole as a purification system for filtering the tar and water. At a specified time interval (every 10 min), part of the gaseous products was sampled to the gas chromatograph for chemical analyses.

Figure 14. Schematic of the experimental setup in the simulated UCG reactor.

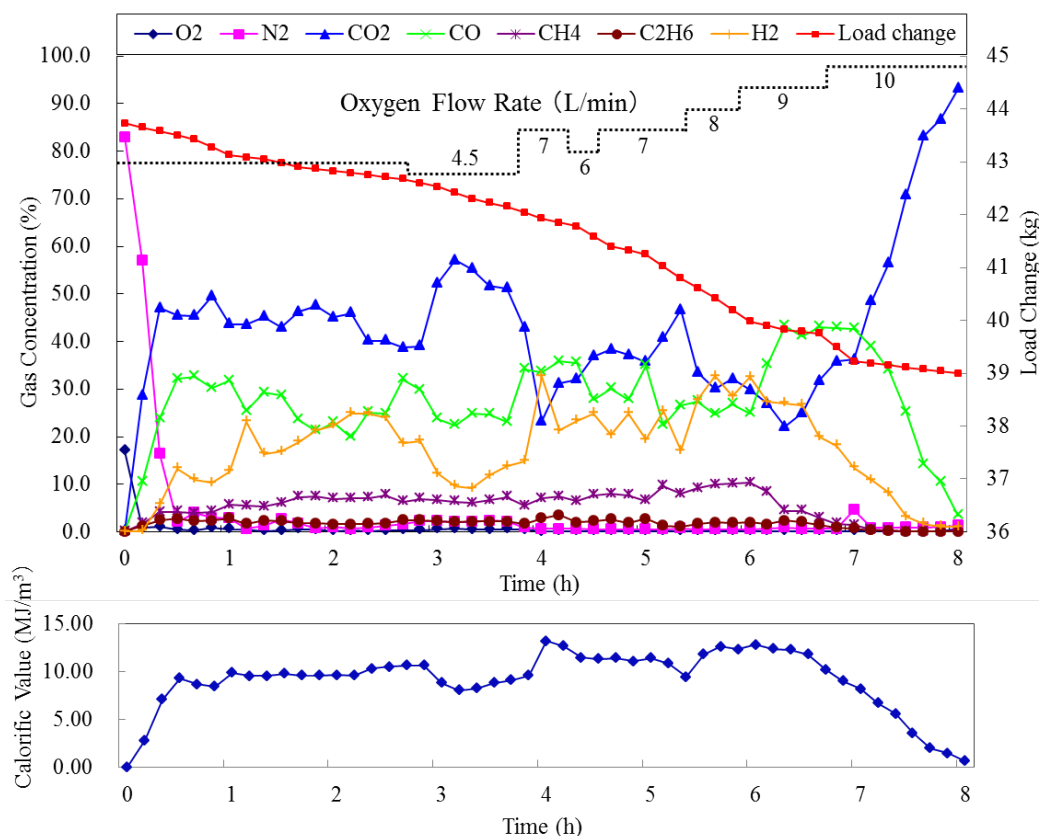
3.4. Results and Discussion

At the start of the experiment, the coal block was ignited by a gas burner in the ignition location, which created a sufficient temperature environment. Then, the oxygen supply system was connected to the inlet position. During the next approximately 8 h, only pure oxygen was supplied to the reaction zone with a flow rate of 4.5–10 L/min to heat up the coal block and to accumulate a sufficient amount of thermal energy for development of the gasification process.

Figure 15 shows the variation of compositions of gas contents and change in weight of the gasifier with respect to the operation time during the experiment. The percentage composition and the calorific value of the gaseous products are presented in the figure, indicating that, in the initial combustion period, the N_2 composition is greater than 80%, which drops gradually along with the CO_2 composition increase.

At about 25 min after beginning the experiment, the gas stream was lit successfully. In the next period of about 3 h, the combustion area displayed a continuous stable gasification. The quality of gas obtained during the phase (3–4 h) was low. It was composed mainly of CO_2 which reached the highest value (57.1%) and the composition of CO , H_2 showed a downward trend. The calculated calorific value of product gas equaled 8.03 MJ/m^3 at this time. Consequently, the oxygen supply rate was increased to 7 L/min; subsequently the CO , H_2 composition exhibited a marked increase. The calorific value also reached the peak value (13.19 MJ/m^3) at 4 h.

Figure 15. Changes in gas production and calorific value, as well as the gasification agent supply rate during the gasification experiment.



After about 7 h, the combustible gas compositions decreased and the ratio of CO₂ continued increasing, despite the improved oxygen supply rate. From the load change in the figure, we can see that the rate of the coal consumed tended to decline at this time. It can be conjectured that the combustion front had moved to the coal block border of gas outlet side and the current oxygen flow rate was too high for stable gasification. The continued increase in the heat carried away with the gas exhaust restricts any further rise of temperature in the reactor. Most gas contents, aside from CO₂, disappeared. As a whole, CO, H₂, and CH₄ are produced continuously throughout the process of experimentation. Analyses of the collected product gas were done using gas chromatography, gas concentrations, and heating values, yielding results presented in Table 4. The average calorific value estimated from these gas contents is about 9.1 MJ/m³.

Table 4. Average gas composition and calorific value of gas products.

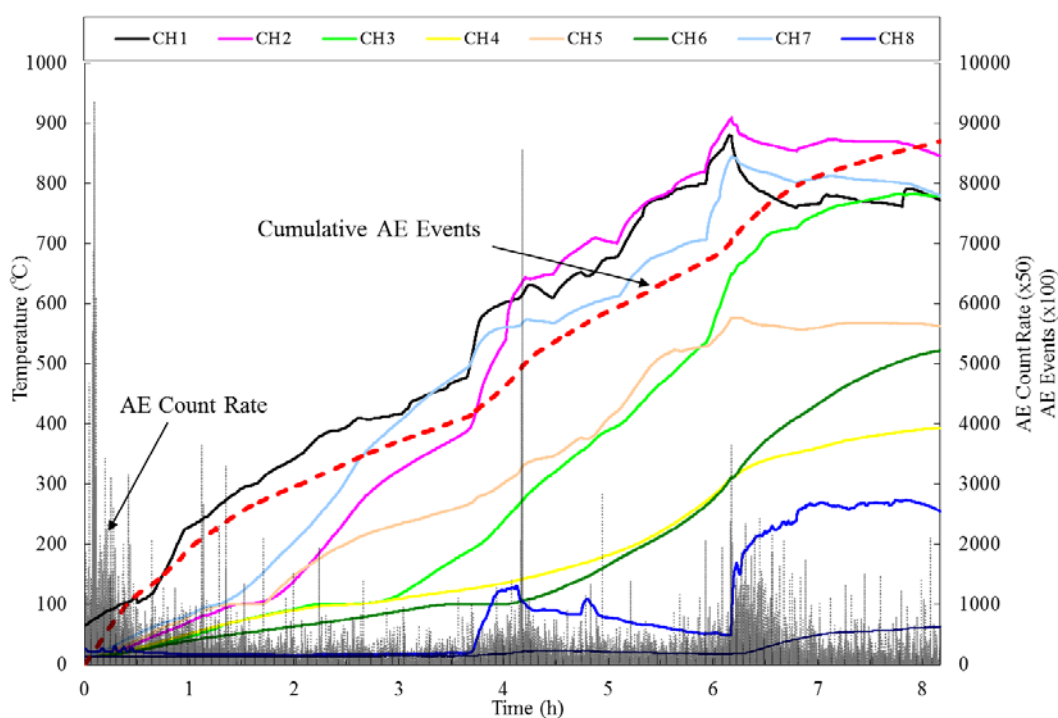
Gas compositions	O ₂ (%)	N ₂ (%)	CO ₂ (%)	CO (%)	CH ₄ (%)	C ₂ H ₆ (%)	H ₂ (%)
Gas concentration	0.6	4.4	43.0	27.5	5.5	1.7	17.2
Calorific value	9.1 MJ/m ³						

Temperature profiles and AE activity inside the model during the experiment are presented in Figure 16. The rates of temperature increase of each thermocouple and the high-temperature areas are clearly visible in this figure. In the gas exhaust passage, the thermocouple CH8 was mounted for detecting the temperatures of gaseous products. The changes in temperature at various locations with

respect to time are visible. During the initial part of the experiment, the temperature around the ignition area (CH1) increased. The higher zone moved along the upper linking-hole (CH2, CH7) in the middle of the period. During the later period, the temperature around the lower linking-hole (CH3, CH6) increased abruptly. Results show that local temperatures rise gradually and reach a level as high as about 900 °C. The highest temperature value is the temperature of the roof of the cavity, wherein combustion occurs. Around this time point, AE count rate and events improved markedly, showing that AE activity increased considerably when the combustion area temperature changed. Corresponding to the same position of 4 h around in Figure 15, the temperature increased sharply and the AE activity also rose after improving the oxygen supply rate. These results show that the gasification process and combustion area are also expanded. After about 6 h of operation, the rate of temperature increase for primary areas of the gasification channel declined gradually, which might show that the reaction zone moved to the coal block border inside the reactor and might indicate termination of the gasification process.

After the experiment, the connecting pipelines were torn down and the plaster was pour into the reactor for observing the cavity shape and cracks. However, the sections were damaged during the cutting operation, because the broken of cavity surrounding and not dry plaster. So we measured the weight shortage before and after the experiment, the total amount of coal consumed in this reactor is about 5 kg for 8h operation. The weight loss maybe also contains of the moisture evaporation within the coal (inherent moisture), the tar, and volatile matters.

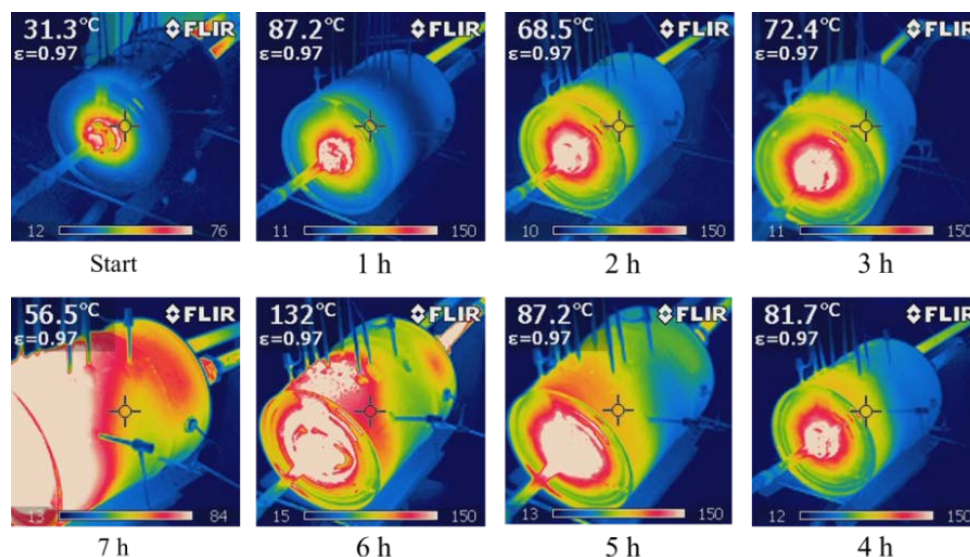
Figure 16. Temperature profile and AE activity monitored during gasification experiment.



The high temperature area photos taken by thermography camera are presented in Figure 17. From these photos, we can clearly see how the combustion area gradually moved with respect to the operation time and can inferred the evolution of the cavity, to some extent.

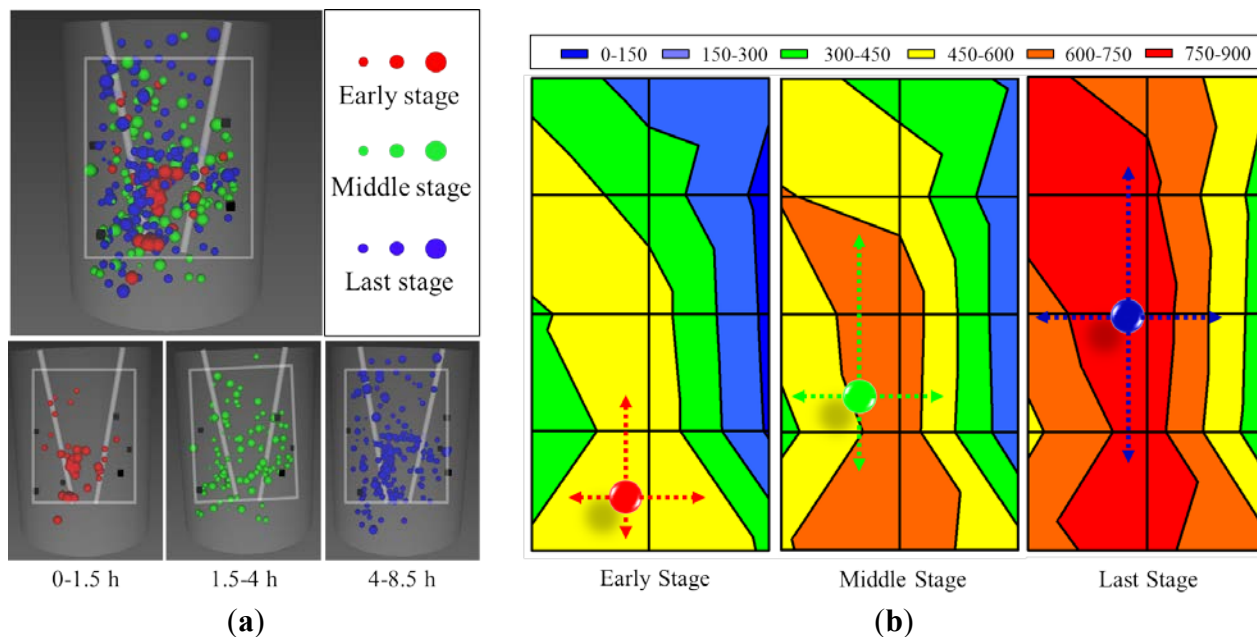
The behavior of the mobile underground burning coal face is ascertained according to the complex interaction between geo-mechanical effects, thermal stress, and combustion state *in situ*. Monitoring and estimating the moving velocity of combustion zone is important for controlling the gasification process effectively. Calculating the time to reach the same temperature as that of thermocouples CH1, CH2, and CH3, the movement rate along the linking hole was estimated roughly as 0.03 m/h, which is an almost identical rate to that of the UCG field measurement [5].

Figure 17. The pictures of cavity growth taken by thermography.



AE signals from sensors CH1–CH6 were also collected using a multi-recorder oscilloscope (GR-7000; Keyence Co., Osaka, Japan) with a sampling time of 10 microseconds. We obtained the triggering time of a microcrack occurring inside the gasifier, which is useful for calculating the source location. Figure 18 depicts the AE source locations: (a) that were obtained by application of the least-squares iteration technique [33] and distribution of the high-temperature area; (b) inside the UCG reactor. Colored dots in Figure 18b express the centers of gravity of the AE cloud, which were calculated using the AE source energies and coordinates projected in the gasifier section. Furthermore, the lengths of arrows in the horizontal and vertical directions represent the breadth of the AE cloud region. Red, green, and blue spheres in Figure 18a respectively depict the AE sources of the early, middle, and later periods. The extent of damage, *i.e.*, energy obtained by cracking, can be differentiated from the sphere sizes. Comparison of the temperature variation and obtained AE source locations (see Figures 16 and 18), as well as the high temperature zone mobile (see Figure 17), reveals a close mutual correlation. It is apparent that the combustion area expanded from the bottom to the central region and that it enlarged around the gasification channel. Positive correlation was found between the temperature change and AE activities generated in the present work. These AEs were generated with crack generation and development along with the local change of temperature inside the model. Most AE sources were located in the ignition area and around the linking-hole, as the figure shows.

Figure 18. (a) AE source locations; (b) Movement of the AE cloud center (high temperature region) inside the gasifier by AE sources and temperature contours.



4. Conclusions

For development of an operational and efficient underground coal gasification system, we conducted coal heating tests with designed setting temperatures to investigate structural changes and other influential factors. An experiment in a laboratory-scale UCG reactor under controlled operating conditions was described. The main conclusions drawn from the present work are the following:

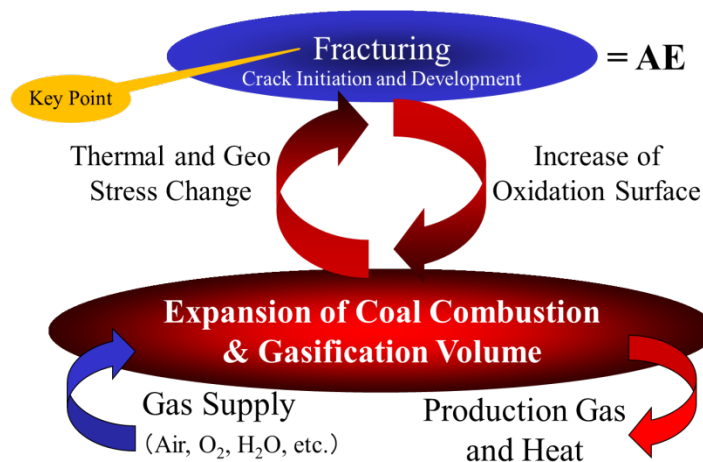
The experiments conducted on coal specimens demonstrated that many microcracks developed inside the coal with AE activity during heating. The temperature gradient and the direction of the stratified plane and fire face affect the crack generation and extension. The crack distribution inside the coal specimens was ascertained through analyses of 3D CT images. Local fractures with AE affect the gasification process parameters, such as the rate of movement of the combustion zone. The obtained results can be useful for UCG simulator construction.

The product gas analysis and temperature profile demonstrate that an appropriately stable performance of the UCG reactor was achieved in this study. Comparison of the temperature variation and accumulated AE event curves revealed a close correlation between them. The correlation coefficient was greater than 0.9. The local change of temperature inside the coal induced fractures with AE. About 5 kg coal was consumed in 8 h. The average calorific value estimated from the product gas was 9.1 MJ/m^3 , which is also the same order as that of field UCG [5].

Results of the present experimental studies demonstrate that effective and sustainable combustion in the underground reactor is necessary in an efficient coal gasification system, which depends on the cavity growth and expansion of gasification volume. Enlargement of the oxidation surface around the gasification channel with crack initiation and development inside the coal seam directly influences the gasification efficiency. Evaluation and control of the fracturing occurring in the gasifier is important for developing an efficient UCG system, as shown in Figure 19. In this figure, the chain reaction of combustion and gasification in coal is explained. The heat of combustion of coal seam induces thermal

stress inside the coal seam. Then cracking occurs, which implies an increased oxidization surface for subsequent combustion: A gasification zone. Therefore, the fracturing activity in the coal seam is a key factor for an efficient UCG system.

Figure 19. Importance of fracturing activity on UCG system.



Future studies are required to try different UCG linking-hole models and research the influence of gasification agents, *i.e.*, the ratios of steam, air and/or oxygen on the gasification effect. Also, the influence of ground water and permeability changes in the coal will be investigated in the future work.

Acknowledgments

This work was supported by the Japanese Society on UCG, Mikasa City, Center of Environmental Science and Disaster Mitigation for Advanced Research of Muroran Institute of Technology and a Grant-in-Aid for Scientific Research (b), 21360441 from the Ministry of Education, Culture, Sports, Science and Technology (MEXT), Japan. The authors gratefully acknowledge their support.

Conflict of Interest

The authors declared that they have no conflicts of interest to this work.

References

1. Energy Information Administration (EIA). *International Energy Outlook 2009*; EIA: Washington, DC, USA, 2009; pp. 49–60.
2. Alexander, Y.K. Early ideas in underground coal gasification and their evolution. *Energies* **2009**, *2*, 456–476.
3. Olness, D.U.; Gregg, D.W. *The Historical Development of Underground Coal Gasification*; Technical Report UCRL-52283; California University, Lawrence Livermore Lab: Livermore, CA, USA, 1977.
4. Betts, A.G. An Improved Process for Utilizing Unmined Coal. UK Patent 21674, filed 1909, issued 1910.

5. Burton, E.; Friedmann, J.; Upadhye, R. *Best Practices in Underground Coal Gasification*; Lawrence Livermore National Laboratory: Livermore, CA, USA, 2006.
6. Kreinin, E.B. Two-stage underground coal gasification. *Coal Chem. Ind.* **1993**, *6*, 61–63.
7. Franke, F.H. Survey on Experiment Laboratory Work on UCG. In Proceedings of the 12th Annual Underground Coal Gasification Symposium, Washington, DC, USA, 21–28 August 1986; pp. 131–133.
8. Yang, L.H.; Liu, S.Q.; Yu, L.; Liang, J. Experimental study of shaftless underground gasification in thin high-angle coal seams. *Energy Fuels* **2007**, *21*, 2390–2397.
9. Thorsness, C.B.; Britten, J.A. *Analysis of Material and Energy Balances for the Rocky Mountain-1 UCG Field Test*; Report No. 44–49. Lawrence Livermore National Laboratory: Livermore, CA, USA, 1984.
10. Debelle, B.; Malmendier, M. Modeling of flow at Thulin underground coal gasification experiments. *Fuel* **1992**, *71*, 95–104.
11. Edgar, T.F. Research and development on underground gasification of Texas lignite. *ACS Symp. Ser.* **1983**, *79*, 66–76.
12. Chandelle, V. The pushing through project of the gasification channel in Tulin coal field. *Min. Technol.* **1992**, *13*, 5–7.
13. Hossein, N.; Mohammad, K.; Zhang, C.; Jalal, A. Simulation study of underground coal gasification in Alberta reservoirs: Geological structure and process modeling. *Energy Fuels* **2010**, *24*, 3540–3550.
14. Alexander, P.; Coats, T.; David, B. Comparative study on the measuring methods adopted in the gasification of horizontal and steep coal layers. *Min. Technol.* **1985**, *5*, 107–115.
15. Collot, A.G. *Prospects for Hydrogen from Coal*; IEA Clean Coal Centre: London, UK, 2003.
16. Stanńczyk, K.; Kapusta, K.; Wiatowski, M.; Świądrowski, J.; Smoliński, A.; Rogut, J.; Kotyrba, A. Experimental simulation of hard coal underground gasification for hydrogen production. *Fuel* **2012**, *91*, 40–50.
17. Barbir, F. *International Association for Hydrogen Energy*; Martinus Nijhoff Publishers: Leiden, The Netherlands, 2009; pp. 275–285.
18. Liang, J.; Liu, S.Q.; Yu, L. Method of stably controlling the process of underground coal gasification. *J. China Univ. Min. Technol.* **2002**, *31*, 358–361.
19. Khadse, A.; Qayyumi, P.; Mahajani, S.; Aghalayam, P. Underground coal gasification: A new clean coal utilization technique for India. *Energy* **2007**, *32*, 2061–2071.
20. Kapusta, K.; Stanńczyk, K. Development conditions and limitations of the underground coal gasification in Poland. *Chem. Rev.* **2009**, *88*, 331–338.
21. Su, F.Q.; Itakura, K.; Deguchi, G.; Ohga, K.; Goto, T.; Yoshida, Y. UCG Laboratory Experiments for Evaluation of Fracturing Activity around Coal Gasification Area. In Proceedings of MMIJ2011, Fall Convention of Mining and Materials Processing Institute, Sakai, Japan, 26–29 September 2011.
22. Buscheck, T.A.; Hao, Y.; Morris, J.P.; Burton, E.A. Thermal–Hydrological Sensitivity Analysis of Underground Coal Gasification. In Proceedings of the 2009 International Pittsburgh Coal Conference, Pittsburgh, PA, USA, 20–23 September 2009.

23. Watanabe, Y.; Itakura, K.; Sato, K.; Fujii, Y.; Balusu, R.; Guo, H.; Luo, X. A Modeling method on fractal distribution of cracks in rocks using AE Monitoring. *J. Acoustic Emiss.* **2005**, *23*, 119–128.
24. Thompson, P.N. Gasifying coal underground. *Endeavour* **1978**, *2*, 2–93.
25. Blinderman, M.S.; Saulov, D.N.; Klimenko, A.Y. Forward and reverse combustion linking in underground coal gasification. *Energy* **2008**, 33–446.
26. Gregg, D.W. Relative merits of alternate linking techniques for underground coal gasification and their system design implications. *In Situ* **1980**, *4*, 207–236.
27. Betts, A.G. *Lead Refining by Electrolysis*; Wiley: New York, NY, USA, 1908.
28. UCG Association. How UCG Works. Available online: <http://www.ucgassociation.org/index.php/home> (accessed on 26 March 2013).
29. Hill, R.W. *The Centralia Partial-Seam CRIP Test*; Lawrence Livermore National Laboratory: Livermore, CA, USA, 1983.
30. Hill, R.W. Review of the CRIP Process. In Proceedings of the Twelfth Annual Underground Coal Gasification Symposium, Saarbrücken, Germany, 21–28 August 1986.
31. Ergo Exergy Technology Incorporated Website. Available online: <http://www.ergoexergy.com> (accessed on 27 March 2013).
32. Thorsness, C.B.; Creighton, J.R. *Review of Underground Coal Gasification Experiments at Hoe Creek*; Report UCRL-87662; Lawrence Livermore National Laboratory: Livermore, CA, USA, 1982.
33. Reginald Hardy, H., Jr. *Acoustic Emission/Microseismic Activity*; Taylor & Francis: Leiden, The Netherlands, 2003.

© 2013 by the authors; licensee MDPI, Basel, Switzerland. This article is an open access article distributed under the terms and conditions of the Creative Commons Attribution license (<http://creativecommons.org/licenses/by/3.0/>).